Science of the Total Environment 649 (2019) 1281–1292

Contents lists available at ScienceDirect

Science of the Total Environment

journal homepage: www.elsevier.com/locate/scitotenv

Hydrochemical properties and chemocline of the Sansha Yongle Blue Hole in the South China Sea

Linping Xie [a], Baodong Wang [a,b,*], Xinming Pu [a], Ming Xin [a], Peiqing He [a], Chengxuan Li [a], Qinsheng Wei [a,b], Xuelei Zhang [a,b], Tiegang Li [a]

[a] The First Institute of Oceanography, State Oceanic Administration, 6 Xianxialing Road, Qingdao 266061, China
[b] Laboratory for Marine Ecology and Environmental Science, Qingdao National Laboratory for Marine Science and Technology, Qingdao 266071, China

HIGHLIGHTS

- Distinct water layers involve different redox/nitrification-denitrification process.
- A 30-m thick chemocline separates the upper oxic layer and the deep anoxic layer.
- The blue hole is a net source of N_2O and CH_4 to the atmosphere.

GRAPHICAL ABSTRACT

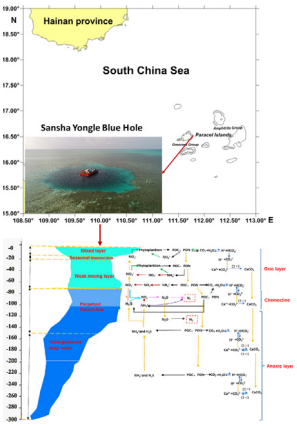

ARTICLE INFO

Article history:
Received 3 July 2018
Received in revised form 24 August 2018
Accepted 24 August 2018
Available online 26 August 2018

Editor: D. Barcelo

Keywords:
Chemocline
Blue hole
Geochemistry
Nitrogen
Carbon
South China Sea

ABSTRACT

Blue holes can provide valuable information regarding paleoclimate, climate change, karst processes, marine ecology, and carbonate geochemistry. The Sansha Yongle Blue Hole, located on Yongle Atoll in the Paracel Islands in the South China Sea, is the deepest blue hole in the world. A comprehensive investigation of the blue hole was conducted to determine the hydrochemical properties and associated redox processes active in the water column. Results indicate the presence of two thermoclines, one at 13–20 m and a second at 70–150 m, dividing the water column into five stratified water layers. Based on redox state, the water column can be divided into three layers: an oxic layer in the top 70 m, a chemocline at 70–100 m, which acts as a redox boundary, and an anoxic deep layer. In the oxic layer, photosynthesis in the oxic layer above the seasonal thermocline, results in nutrient uptake, transformation of inorganic carbon to organic carbon in the top mixed layer above the seasonal thermocline; Below the seasonal thermocline, organic matter degradation and nitrification, which are the main biological process at depths around 30 m and 50–70 m, lead to the accumulation of nitrate and a decrease in dissolved oxygen and pH; whereas photosynthesis is dominant at depths of 30–50 m, leading to increase in dissolved oxygen and pH. Within the chemocline, organic matter decays via a variety of reactions (e.g. aerobic mineralization, denitrification and anammox), leading to sharp decreases in the oxidizing chemical species (e.g., dissolved oxygen and nitrate) and corresponding increases in the reduced species (e.g., ammonium and

* Corresponding author at: First Institute of Oceanography, State Oceanic Administration, 6 Xianxialing Road, Qingdao, China.
E-mail address: wangbd@fio.org.cn (B. Wang).

https://doi.org/10.1016/j.scitotenv.2018.08.333

sulfide). Within this layer, about 60% of the nitrogen is lost and chemoautotrophic/photoautotrophic production may contribute significantly to particulate organic carbon. Within the deep anoxic layer, sulfate reduction and degradation of organic matter result in accumulations of sulfide, dissolved inorganic carbon, and nutrients.

1. Introduction

Over the past 50 years, blue holes have been widely studied as potential time capsules containing records of Earth's past climate and climate changes (Mylroie et al., 1995; Kjellmark, 1996; Schwabe and Herbert, 2004). The core from the Church Blue Hole suggests that a late Holocene dry period occurred that may correlate to the widespread dry period in the Caribbean between 3200 and 1500 cal yr BP (Kjellmark, 1996). Additionally, blue hole may provide information regarding karst processes, marine ecology, and carbonate geochemistry (Mylroie et al., 1995; Schwabe and Herbert, 2004;). Such information is especially valuable in light of present climate changes and global warming.

Oceanic blue holes originally formed as limestone caves during the last glacial period, when sea level was 100–120 m below the current level (Hatcher, 2006). They typically consist of horizontal cave passages that extend under the sea floor as deep, vertical cracks that run parallel to the edges of carbonate platform (Gonzalez, 2010). Blue holes may contain multiple pycnoclines, which are associated with complex physicochemical profiles (Seymour et al., 2007). Typically, blue holes contain tidally influenced, but vertically stratified, water column of fresh and salt water (Martin et al., 2012). Thus, the water column can be divided into three layers: the upper tidally influenced layer of freshwater, the halocline hypoxic layer typically characterized by corrosive reactions, and the bottom layer of saltwater (Vermette and Hudson, 2001; Martin et al., 2012). Other systems, such as anchialine caves, usually have notable oxic/anoxic interfaces due to the presence of a permanent thermo-halocline. Haloclines are areas of increased limestone dissolution (Pohlman et al., 1997), and hydrogen sulfide usually forms below or at the halocline (Pohlman et al., 1997).

Blue holes differ from other marine habitats in that they have little photosynthetic oxygen production and restricted vertical mixing. These unique hydrobiochemical characteristics result in anoxic conditions and biogeochemical cycling that differs strongly from that taking place in other marine environments (Gonzalez et al., 2011). As a result, bacterial primary production contributes significantly to blue-hole food webs (Macalady et al., 2008; Gonzalez et al., 2011). Variability in geological, hydrological, and chemical characteristics such as the passage configuration and salinity stratification has yielded a great diversity of blue-hole systems around the world. These systems are isolated natural laboratories that have the potential to reveal fundamental relationships between living organisms and biogeochemical environments, both in the currently and as potential analogs for stratified ocean conditions that were likely prevalent earlier in Earth's history (Gonzalez et al., 2011).

The Sansha Yongle Blue Hole (also called Dragon Hole) in the South China Sea is the deepest blue hole in the world. It has attracted the attention of explorers and scientists in recent years because of its unique properties such as the lack of fresh water injection or subsurface connection to the sea and the presence of anoxic deep water. To date, the hydrochemical properties of the water column contained in the Sansha Yongle Blue Hole have not yet been documented in detail because of the difficulties associated with accessing the blue hole with a large observation platform or conducting sampling within its sinuous underwater structure. Using a large anchored floating platform and advanced observation equipment including a remotely operated vehicle (ROV), we carried out a comprehensive investigation of the Sansha Yongle Blue Hole in May 2017. This paper reports the hydrochemical properties of the water column contained within the blue hole, emphasizing the structure of the chemocline. The objectives of this study are to clarify the geochemical processes of nitrogen and carbon in the blue hole.

2. Materials and methods

2.1. Study sites

The Sansha Yongle Blue Hole is located on Yongle Atoll, Paracel Islands, South China Sea (Fig. 1a, b). It is about 300 m deep, and is almost 100 m deeper than the second deepest blue hole–Dean's Blue Hole, located in a bay west of Clarence Town on Long Island, Bahamas (Gischler, 2011). Other blue holes are about half as deep as the Sansha Yongle Blue Hole, with depths of around 100–120 m (Flynn, 2013; Naumann et al., 2015). The Sansha Yongle Blue Hole is shaped like a vertically-held ballet shoe, with the diameter varying from ~130 m at the surface to ~32 m at the bottom. Its central axis runs from southwest to northeast. From the surface to a depth of 124 m, the blue hole remains vertical. It then extends the northeast between the depths of 124 m and ~160 m, below which it turns again, becoming subvertical toward the bottom (Fig. 1c).

2.2. Sampling and chemical analyses

Sampling was performed in May 2017 on an anchored working platform, on board R/V *Changhe Ocean*, as well as on a boat located at six stations inside and outside the blue hole (Fig. 1). High-resolution sampling was carried out inside the blue hole. Samples from the upper water column of the blue hole were collected using a 12-bottle rosette sampler deployed from an anchored working platform, whereas deep water samples (below 130 m) were collected using a ROV equipped with Go-Flo bottles. At deep stations located outside the blue hole (C3 and C4), samples were collected from on board the R/V *Changhe Ocean* using the same rosette sampler that was used to collect shallow water inside the blue hole. At shallow stations located outside the blue hole (C1, C2 and C5), samples were collected using a Go-Flo sampler deployed from a boat.

2.2.1. Temperature, salinity, dissolved oxygen, sulfide and oxidation–reduction potential analyses

Profiles of temperature, salinity, density and dissolved oxygen (DO) were determined using a SED 911 plus conductivity–temperature–depth (CTD) unit and DO sensor manufactured by Sea-Bird (America). The DO sensor was pre-calibrated against air-saturated pure water and post-calibrated using simultaneous discrete Winkler DO data. Salinity measurements are reported using practical salinity units (PSS-78) derived from electrical conductivity measurements. The DO sensor was pre-calibrated against air-saturated pure water and post-calibrated using simultaneous discrete Winkler DO data. Discrete dissolved oxygen was measured with a Metrohm 848 Titrino plus sensor using the Winkler method (Metrohm, Switzerland) (Chen et al., 2001). Analytical precision of DO determination is estimated to be approximately 0.32% at the 190 μmol L^{-1} level (Chen et al., 2001). Sulfide samples collected from the Nisken bottles were immediately fixed in situ with zinc acetate. Sulfide content was measured in an onshore laboratory using the methylene blue method with a precision of 7.6% at the

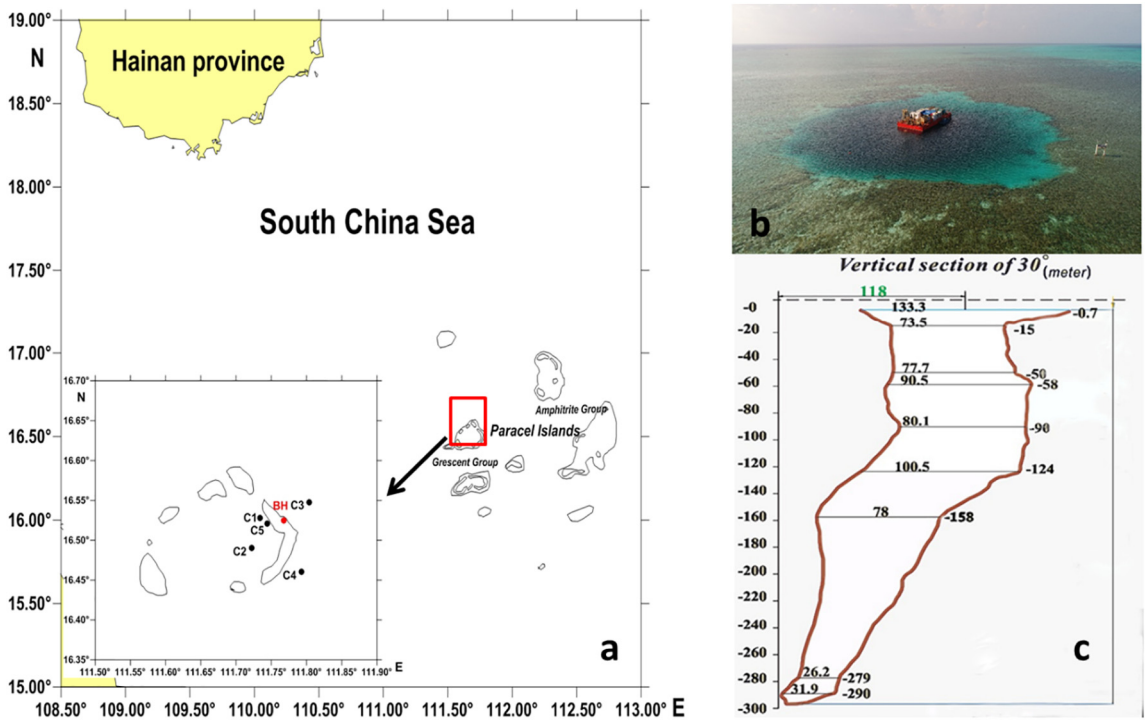

Fig. 1. (a) Location of the Sansha Yongle Blue Hole. Red and black dots indicate locations of sampling stations inside and outside the blue hole, respectively. (b) Bird's-eye view of the Sansha Yongle Blue Hole. (c) Vertical section through the Sansha Yongle Blue Hole. (For interpretation of the references to colour in this figure legend, the reader is referred to the web version of this article.)

427 μg L^{-1} level (State technology supervision bureau, 2007). Oxidation–reduction potential (ORP) was measured with the potentiometric method (State technology supervision bureau, 2007).

2.2.2. Nutrients and suspended particulate matter (SPM) analyses

Water samples were immediately filtered through 0.45-μm cellulose-acetate filters. Both the filtrate (for nutrients analyses) and filter membrane (for SPM analyses) were stored at −20 °C. Nitrite (NO_2^-), nitrate (NO_3^-), ammonium (NH_4^+), silicate (SiO_3^{2-}), and phosphate (PO_4^{3-}) were analyzed using colorimetric methods with a QuAAtro nutrient automatic analyzer (Bran + Luebbe Gmbh, Germany) in an onshore laboratory. Nitrate and NO_2^- were determined by the standard pink azo dye method (Strickland and Parsons, 1972), and NH_4^+ was measured by the hypobromite oxidation method with precisions of 0.30 μmol L^{-1}, 0.02 μmol L^{-1}, and 0.1 μmol L^{-1}, respectively (Strickland and Parsons, 1972). Phosphate was determined using the molybdenum blue method (Murphy and Riley, 1962; Su-Cheng et al., 1990) with a precision of 0.5% at 2.8 μmol L^{-1} and 3% at 0.1 μmol L^{-1}; SiO_3^{2-} was measured with the molybdosilicic acid method (Fanning and Pilson, 1973) with a precision of 0.6% at 150 μmol L^{-1} and 2% at 5 μmol L^{-1}. Suspended particulate matter concentrations were obtained by gravimetric analysis. Dissolved inorganic nitrogen (DIN) is the sum of NO_3^-, NO_2^- and NH_4^+ concentrations.

2.2.3. Biogenic gases

Samples for nitrous oxide (N_2O) and methane (CH_4) collected from Nisken bottles were preserved with saturated $HgCl_2$ and stored in a cooled dark chamber at 4 °C. N_2O and CH_4 were measured at the Ocean University of China by gas chromatography using gas-stripping methods (Zhang et al., 2004, 2006). The precisions of the determination of N_2O and CH_4 are 5% and 3%, respectively.

2.2.4. Organic carbon and carbonate system

Samples were filtered through pre-combusted glass-fiber filters. Both the filtrate and filter membrane were stored at −20 °C for dissolved organic carbon (DOC) and particulate organic carbon (POC) analyses, respectively. Concentrations of DOC were measured by high-temperature catalytic oxidation using a Total Organic Carbon analyzer (Shimadzu, Japan) (Sugimura and Suzuki, 1988). The precision of DOC analyses is ~1 μmol L^{-1}. The concentration of POC on the filters was measured using a CHN elemental analyzer (Elementar Analysensysteme GmbH, Germany). These analyses have a mean error of 0.02% for every 10 measurements of the same sample and a relative standard deviation of <10%. Dissolved inorganic carbon (DIC) samples were preserved with saturated $HgCl_2$ and stored in a cooled dark chamber at 4 °C. Dissolved inorganic carbon was measured shortly after the cruise by acidifying 0.5 mL of sample and quantifying of carbon dioxide (CO_2) concentration using a DIC analyzer (Apollo SciTech, America). The method has a precision of 0.1% to 0.2% in coastal water (Cai and Wang, 1998). A potentiometric pH sensor (Thermo Fisher Orion, America) was used to determine pH values using the National Bureau of Standards (NBS) scale. Values were then corrected to reflect in situ temperature and salinity conditions. The sensor has a precision of ±0.1 in pH units.

To better understand the carbonate system of the blue hole, the partial pressure of carbon dioxide (pCO_2), and the saturation states of calcite (Ω_{Ca}) and aragonite (Ω_{Ar}) were calculated at in situ temperature, salinity, and pressure conditions from pH, DIC, PO_4^{3-} and SiO_3^{2-} data using the CO_2SYS program of Pierrot et al. (2006) configured for Excel. The set of apparent dissociation constants of carbonic acid (K_1 and K_2) of Lueker et al. (2000), the sulfate constants of Dickson (1990), and the borate constant of Uppström (1974) were used.

2.3. Calculation of the air-sea flux of biogenic gases

Fluxes of N_2O and CH_4 from the sea surface to the atmosphere were calculated using the following equation:

$$F = k_w \times (C_{obs} - C_{eq}) \quad (1)$$

where F is the flux (mol m^{-2} d^{-1}); k_w is the gas transfer velocity coefficient in cm h^{-1}, which was calculated using the tri-linear k/wind speed relationship established by Liss and Merlivat (1986) (LM86)

and the quadratic k/wind speed relationship established by Wanninkhof (1992) (W92). LM86 and W92 are often assumed to define the lower and upper limits of k_w. C_{obs} is the observed concentration of dissolved gases (nmol L^{-1}); C_{eq} is concentration of N_2O or CH_4 in seawater that in equilibrium with the atmosphere (nmol L^{-1}), which was calculated for the in situ temperature and salinity using the solubility data of Wiesenburg and Gulnasso Jr (1979) and Weiss and Price (1980), respectively. C_{eq} was calculated using the annual average atmospheric concentrations of N_2O and CH_4 measured at Mauna Loa (Hawaii, United States) and reported as part of the NOAA/ESRL halocarbons in situ program (http://www.esrl.noaa.gov/gmd). In 2017, these values were 330 ppb and 1860 ppb for N_2O and CH_4, respectively. The major uncertainty in assessing sea-to-air gas fluxes is related to the estimation of the gas transfer coefficient, which depends on the type of wind data used. In this work, we computed the gas transfer coefficients using the in situ wind speeds measured by a wind monitor, which ranged from 4.60 to 9.80 m s^{-1} with an average of 6.98 ± 0.88 m s^{-1}.

N_2O and CH_4 saturations were calculated using the following equation:

$$R\% = (C_{obs}/C_{eq}) \times 100 \quad (2)$$

where R is saturations of N_2O or CH_4; C_{obs} is the observed concentration of dissolved gases (nmol L^{-1}); C_{eq} is concentration of N_2O or CH_4 in seawater that in equilibrium with the atmosphere (nmol L^{-1}), which was calculated for the in situ temperature and salinity using the solubility data ofWiesenburg and Gulnasso Jr (1979) and Weiss and Price (1980), respectively.

3. Results

3.1. Main hydrological features

The Sansha Yongle Blue Hole was found to be a strongly stratified system in which the water column was divided into five distinct layers by two thermoclines (Fig. 2a). The upper mixed layer (the top ~13 m) was characterized by the highest temperature and lowest salinity. The seasonal thermocline was located at a depth of 13–20 m, where temperature decreased from approximately 30 to 26 °C whereas salinity increased from 33.38 to 33.68. Below the seasonal thermocline was a weak mixing layer at a depth of 20–70 m with a temperature of approximately 25 °C and a salinity of approximately 33.8. The permanent thermocline was located at a depth of 70–150 m, where the temperature decreased sharply from 24.2 to 15.7 °C and salinity increased from 33.96 to 34.50. The deepest layer of the water column was nearly homogeneous with depth, exhibiting only a slight increase in temperature but constant salinity.

The hydrological structure of the water column inside the blue hole was different from that outside the blue hole. At the deep station C4, located outside the blue hole, there was only one seasonal thermocline at a depth of 27–37 m, which was deeper than the one inside the blue hole. Additionally, the subsurface water characterized by salinity maximum (up to 34.7) in the open South China Sea was not found inside the blue hole. The water column inside the blue hole was much more stable, possibly due to the blue hole's narrow diameter and the blocking effect of Yongle Atoll (Fig. 2b).

3.2. Dissolved oxygen, sulfide and oxidation–reduction potential

Dissolved oxygen in surface water was almost at saturation. However, DO concentration decreased sharply from >233 μmol L^{-1} at the surface to nearly half that value (~130 μmol L^{-1}) at the lower boundary of the seasonal thermocline. Within the weak mixing layer below the seasonal thermocline, DO concentration increased slightly from ~132 μmol L^{-1} to ~158 μmol L^{-1} at a depth of 50 m. DO concentrations then decreased sharply again in the permanent thermocline and were undetectable level at a depth of 90 m. Sulfide was detectable at a depth of 80 m but remained at low level (<1.0 μmol L^{-1}) until a depth of 90 m. Sulfide concentration increased almost linearly from ~10 μmol L^{-1} at a depth of 100 m to ~45 μmol L^{-1} at a depth of 150 m, or the bottom of the permanent thermocline, and maintained this level all the way to the bottom of the water column. In addition, ORP, which reflects the redox state of the water, was positive above 80 m but decreased sharply to −169 mV at 90 m; ORP was approximately ~ −300 mV in the deep anoxic water. The deep anoxic water mass accounted for two-thirds of the volume of the entire water column (Fig. 3a).

Below the oxic surface and above the anoxic deep water, there was a layer with both very little oxygen (<20 μmol L^{-1}) and little sulfide (<1 mol L^{-1}). This “suboxic layer” is approximately 10 m thick and lies between the depths of 90 and 100 m. Within the blue hole, oxygen and sulfide were found to coexist over a depth of about 20 m.

The profile of DO at station C4 outside the blue hole was similar to that measured in the temperate open ocean but quite different from that measured inside the blue hole (Fig. 3b). Outside the blue hole, a subsurface oxygen maximum was observed at depths of 30–50 m, formed by phytoplankton photosynthesis at the subsurface chlorophyll maximum layer. Outside the blue hole, sulfide was undetectable in the water column and ORP was positive, increasing slightly with depth (Fig. 3b).

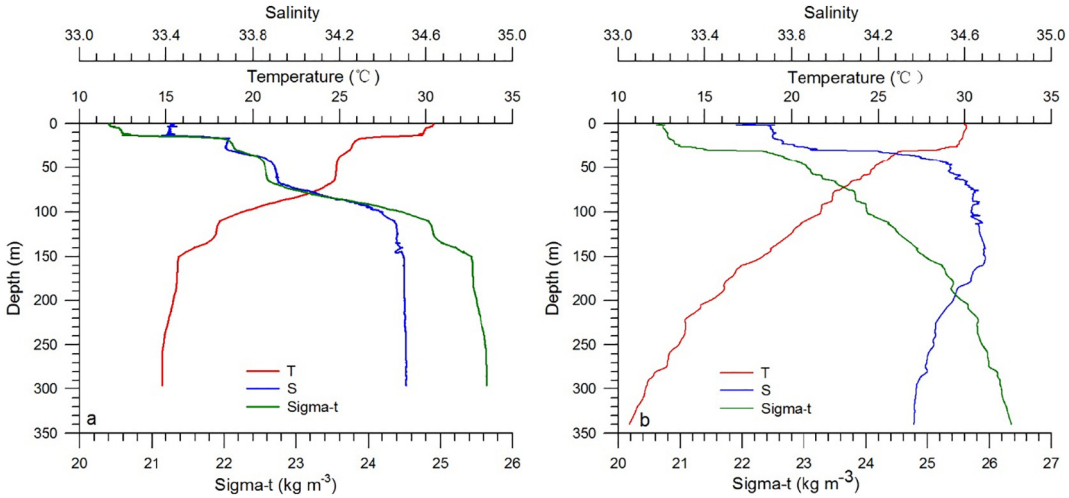

Fig. 2. Profiles of seawater temperature, salinity and Sigma-t (a) inside and (b) outside the Sansha Yongle Blue Hole in May 2017.

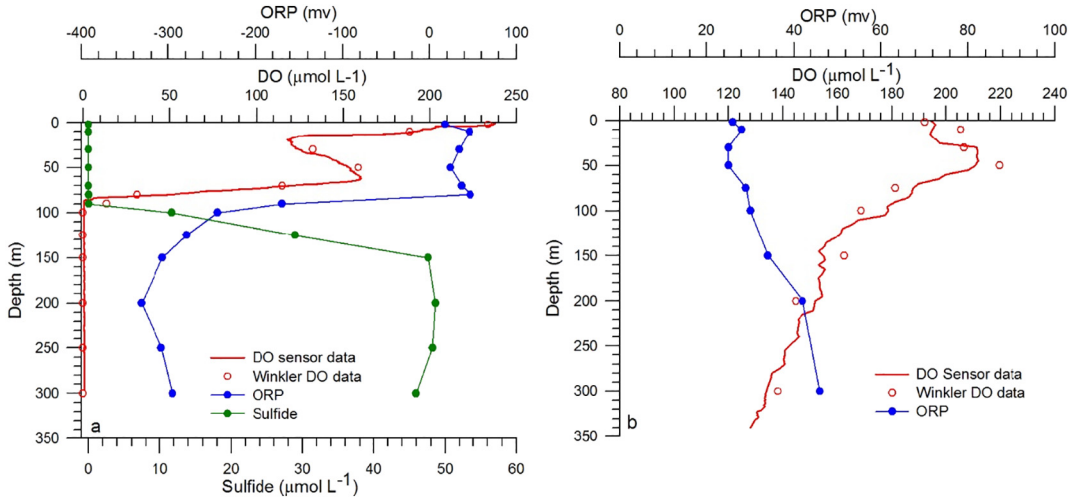

Fig. 3. Profiles of dissolved oxygen (DO) (red line represents DO sensor data calibrated using simultaneous discrete Winkler DO data and red hollow circles represent discrete Winkler DO data), Oxidation–Reduction Potential (ORP) and sulfide (a) inside and (b) outside the Sansha Yongle Blue Hole in May 2017. (For interpretation of the references to colour in this figure legend, the reader is referred to the web version of this article.)

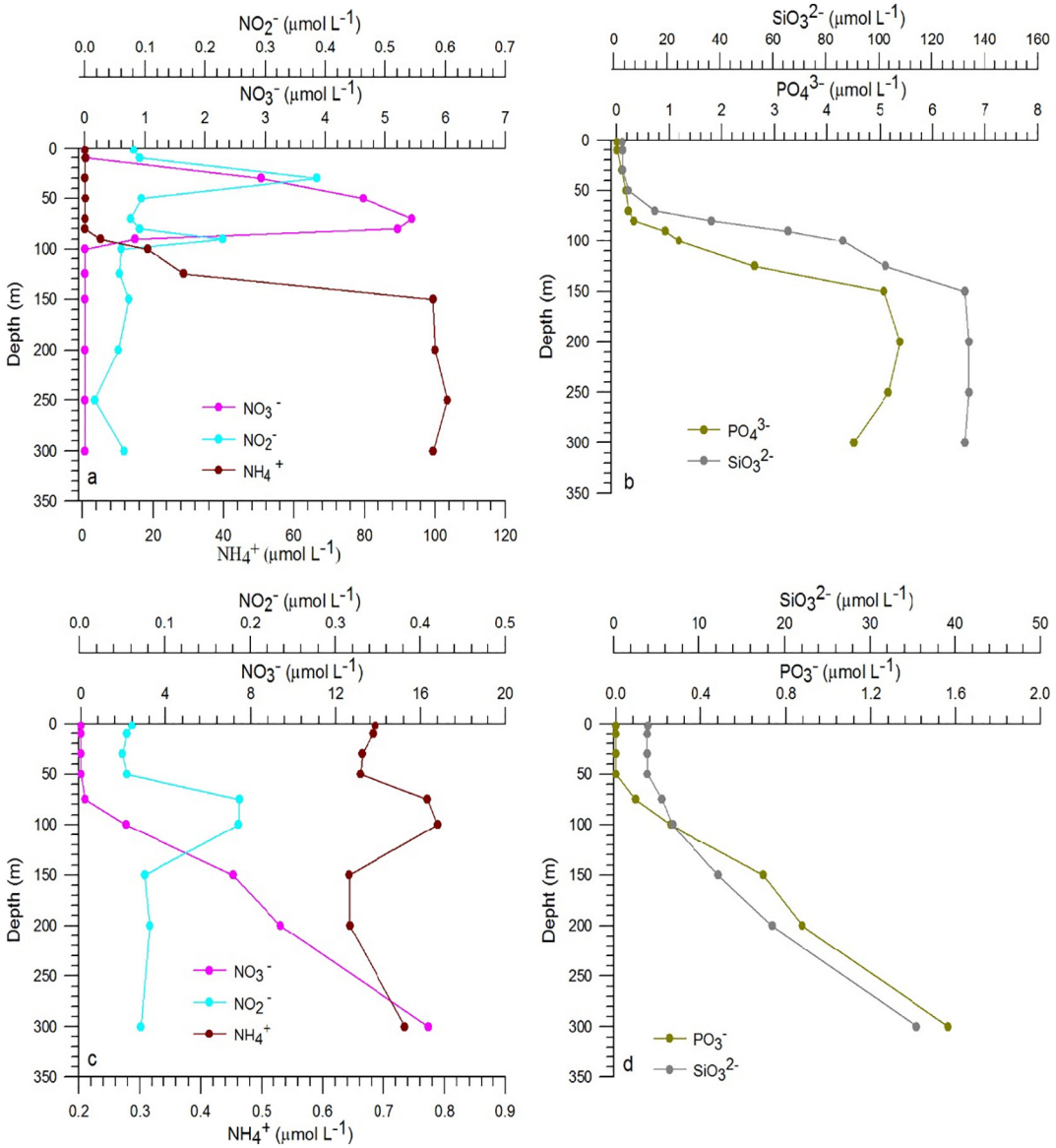

Fig. 4. Profiles of nitrate (NO_3^-), nitrite (NO_2^-), ammonium (NH_4^+), phosphate (PO_4^{3+}), and silicate (SiO_3^{2-}) (a, b) inside and (c, d) outside the Sansha Yongle Blue Hole in May 2017.

3.3. Nutrients

In the blue hole, DIN was very low in the upper mixed layer due to biological uptake. Within and below the seasonal thermocline, NO_3^- increased sharply as a result of respiration via aerobic decomposition of organic matter (nitrification). It reached a maximum of 5.44 μmol L^{-1} at a depth of about 70 m. Within the permanent thermocline, however, nitrate sharply decreased from 5.22 μmol L^{-1} to un detectable levels at a depth of 100 m (Fig. 4 a). Concentrations of NO_2^- were low in both the upper mixed layer and the deep water, but there was a primary maximum (up to 0.4 μmol L^{-1}) at a depth of about 30 m, below the seasonal thermocline, and a secondary maximum within the suboxic zone. Ammonium was depleted in the upper mixed layer, but NH_4^+ concentrations increased within the suboxic layer and reached a maximum of ~100 μmol L^{-1} in the deep water. In the deep anoxic water, NH_4^+ was determined to be the dominant form of DIN (>99.9%).

Concentrations of PO_4^{3-} and SiO_3^{2-} were very low in the upper mixed layer due to phytoplankton uptake. Their concentrations started to increase at a depth of 30 m and increased more sharply at a depth of 70 m, reaching a maximum at a depth of ~150 m and maintaining nearly constant levels throughout the anoxic deep water (Fig. 4b).

The vertical structures of nutrients in the water column at station C4, located outside the blue hole, were similar to those found in the open ocean (Fig. 4c). Nutrients were depleted in the surface mixed layer. Below 75 m, NO_3^- concentration increased with depth. Maximum values of NH_4^+ of ~0.79 μmol L^{-1} were recorded at depths of 75–100 m, and were accompanied by peaks in NO_2^- concentration, which were on the order of 0.19 μmol L^{-1}. The NO_2^- peaks were probably due to nitrification and phytoplankton excretion. Both NH_4^+ and NO_2^- concentrations changed little above 50 m and below 150 m. Profiles of PO_4^{3-}, SiO_3^{2-}, were similar to those for NO_3^- throughout the entire water column (Fig. 4d).

3.4. Biogenic gases

3.4.1. Vertical distributions of N_2O and CH_4 in the water column

In the blue hole, N_2O concentrations exhibited a small maximum at a depth of 30 m, which coincided with the primary nitrite maximum and was located directly above the NO_3^- maximum. Below the lower boundary of the oxycline, N_2O concentration decreased sharply from 8.4 to ~3.0 nmol L^{-1} at the onset of the anoxic water before becoming undetectable in the deep anoxic water. Low concentrations (<9 nmol L^{-1}) of CH_4 were present in the oxic layers, and CH_4 concentrations increased with depth below the suboxic layer, in concert with sulfide and NH_4^+. Concentration of CH_4 increased from ~100 nmol L^{-1} in the suboxic layer to 340 nmol L^{-1} in the upper anoxic water (at a depth of 125 m), and then increased sharply to ~2400 nmol L^{-1} at 150 m before reaching ~2700 nmol L^{-1} in the bottom water (Fig. 5a).

Profiles of N_2O and CH_4 measured at station C4 outside the blue hole are shown in Fig. 5b. The mean concentration of N_2O was 8.5 nmol L^{-1}, which was similar to that measured in the oxic water of the blue hole. A small peak was observed near a depth of 150 m, directly below the maxima for NO_2^- and NH_4^+. The mean concentration of CH_4 was 6.60 nmol L^{-1}, which was similar to that in the oxic water of the blue hole. Higher CH_4 concentrations were observed in the surface water, and a CH_4 maximum located at the base of the mixed layer is a common open-ocean feature that appears to be a result of reactions accompanying grazing (Reeburgh et al., 1991).

3.4.2. Sea-to-air fluxes of N_2O and CH_4

In the blue hole, the N_2O concentration in the surface water (~2 m below the sea water) was 7.37 nmol L^{-1} with a saturation value of 129%. The flux of N_2O to the atmosphere estimated to be 4.87 μmol m^{-2} d^{-1} using the LM86 equations, and 7.53 μmol m^{-2} d^{-1} using the W92 equations. Concentration of CH_4 in the surface water was 8.49 nmol L^{-1} with a saturation value of 453%. The sea-to-air flux of CH_4 was estimated to be 19.7 μmol m^{-2} d^{-1} based on the LM86 equations, and 30.4 μmol m^{-2} d^{-1} based on the W92 equations. Outside the blue hole, at stations C1–C5, the average concentrations of N_2O and CH_4 in the surface waters were 6.84 nmol L^{-1} and 6.53 nmol L^{-1}, respectively. Surface waters were supersaturated with respect to N_2O and CH_4.Using the LM86 equations, estimated sea-to-air fluxes of N_2O and CH_4 ranged from 2.66 to 4.35 μmol m^{-2} d^{-1} and from 12.3 to 17.4 μmol m^{-2} d^{-1} respectively. Using the W92 equations, estimated fluxes to the atmosphere ranged from 3.89 to 6.73 μmol m^{-2} d^{-1} for N_2O and from 17.0 to 25.5 μmol m^{-2} d^{-1} for CH_4.

3.5. Organic carbon and the carbonate system

Profiles of SPM and variables in the carbon system (DOC, POC, pH, and DIC) of the blue hole are shown in Fig. 6a, b. Concentrations of SPM were low and varied little with depth, but there was a maximum within the suboxic layer (at a depth of 90 m). There were two characteristic maxima of POC: one was located at a depth of 30 m and the other at 80 m. The POC profile was uniform below the permanent thermocline. Concentrations of DOC exhibited a subsurface maximum at 70 m and a deep maximum at 150 m.

Profiles of carbonate variables in the blue hole showed distinct characteristics (Fig. 6b, Fig. 7a). The value of pH was 8.09 in the surface water, but decreased to 7.93 at a depth of 30 m, where there was a DO minimum due to respiration. At 50 m, pH increased to 8.00, where there was a DO maximum due to photosynthesis by phytoplankton and filamentous green algae attached to the wall of the cave. Below

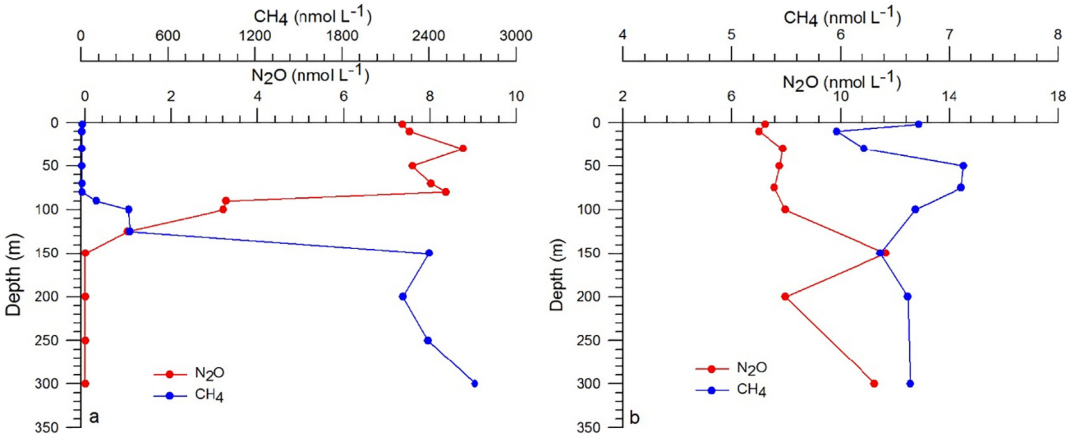

Fig. 5. Profiles of nitrous oxide (N_2O) and methane (CH_4) (a) inside and (b) outside the Sansha Yongle Blue Hole in May 2017.

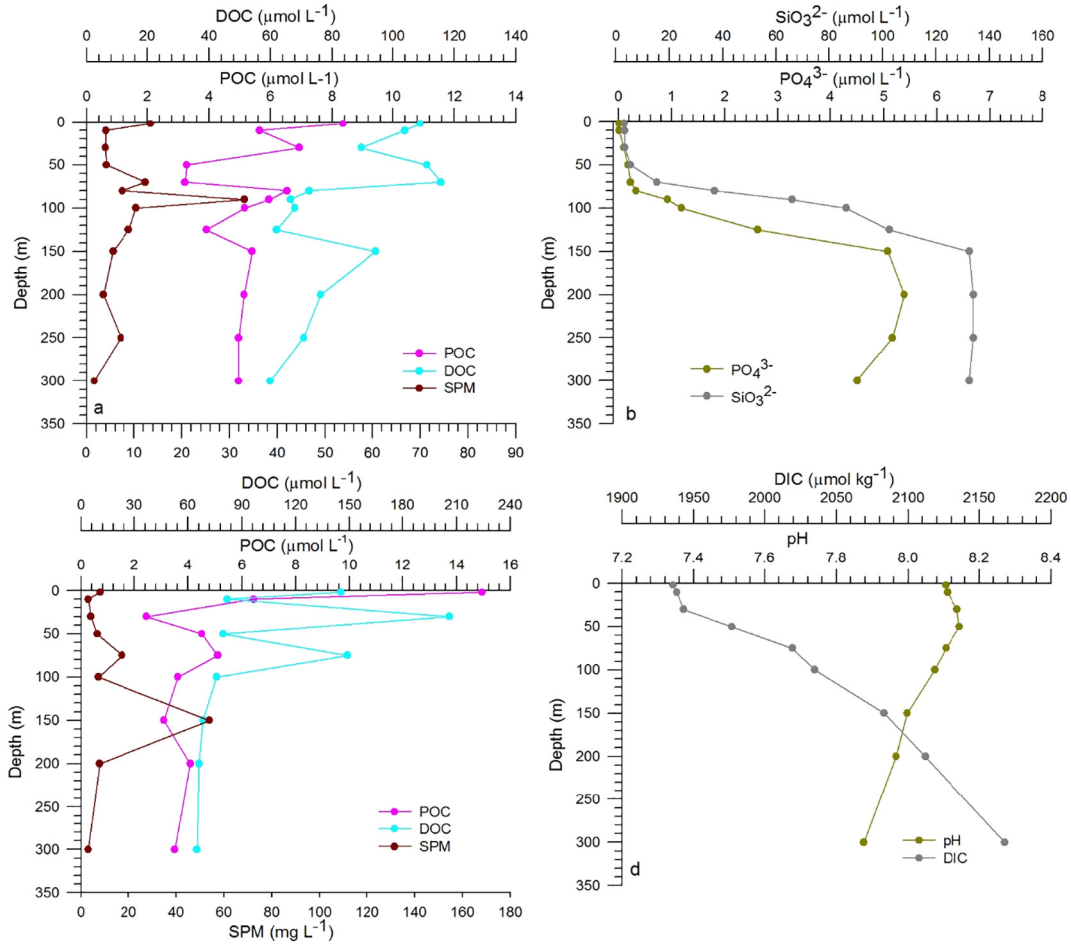

Fig. 6. Profiles of suspended particulate matter (SPM), particulate organic carbon (POC), dissolved organic carbon (DOC), pH, and dissolved inorganic carbon (DIC) (a, b) inside and (c, d) outside the Sansha Yongle Blue Hole in May 2017.

50 m, pH decreased sharply to 7.67 in the suboxic layer (at a depth of 90 m) and was at 7.49 in the anoxic deep water. Unlike the complicated profile of pH, DIC increased with depth throughout the entire water column. The gradient of the DIC profile reached a maximum in the permanent thermocline. Much smaller profile gradients were observed in the upper 70 m of the water column as well as below 150 m.

Fig. 7a plots the calculated pCO_2, Ω_{Ca} and Ω_{Ar} versus depth. The increase in pCO_2 coincides with a decrease in pH. The saturation states of both calcite (Ω_{Ca}) and aragonite (Ω_{Ar}) decreased with depth. In the anoxic water below a depth of 100 m, Ω_{Ar} was close to 1, whereas, Ω_{Ca} was roughly 1.5, indicating potential dissolution of aragonite within the anoxic deep water.

Outside the blue hole, at station C4, the mean value of SPM was slightly higher than that measured inside the blue hole. A SPM maximum was observed at a depth of about 150 m (Fig. 6b). Concentrations of POC decreased sharply with depth within the upper mixed layer,

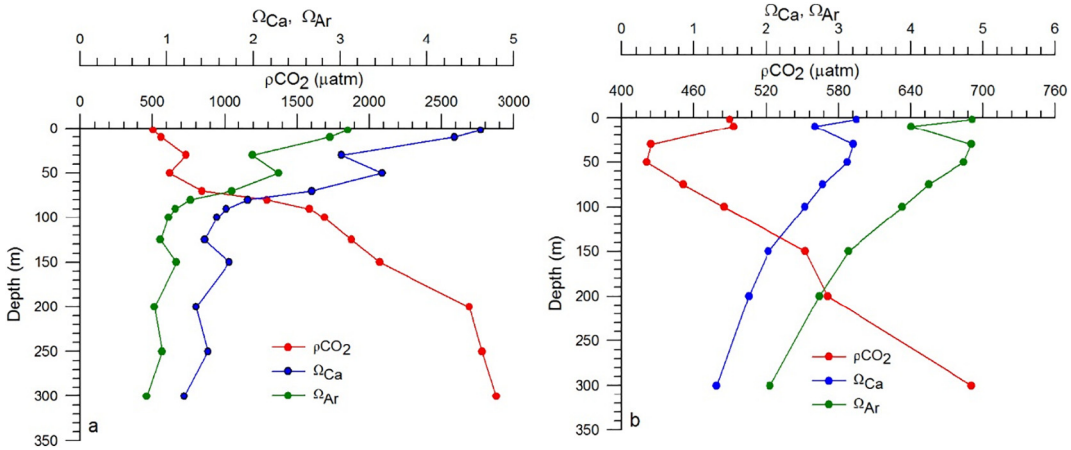

Fig. 7. Profiles of calculated partial pressure of carbon dioxide (p_{CO2}), saturation states of calcite (Ω_{Ca}) and aragonite (Ω_{Ar}) (a) inside and (b) outside the Sansha Yongle Blue Hole in May 2017.

Table 1
Concentrations of chemical variables inside and outside the Sansha Yongle Blue Hole. Arithmetic means and relative standard deviation are presented.

Stations	DO	Sulfide	ORP	SiO_3^{2-}	PO_4^{3-}	NO_3^-	NO_2^-
The oxic layer inside the blue hoe	165.72 ± 47.13	/	31.80 ± 11.01	6.16 ± 5.25	0.10 ± 0.10	2.60 ± 1.53	0.15 ± 0.13
The chemocline inside the blue hoe	22.20 ± 12.47	0.02 ± 0.01	−61.00 ± 152.74	51.34 ± 20.56	0.63 ± 0.42	3.02 ± 3.10	0.16 ± 0.10
The anoxic layer inside the blue hoe	/	38.51 ± 15.12	−294.00 ± 29.87	120.25 ± 20.67	3.99 ± 1.71	0.01 ± 0.00	0.05 ± 0.02
Deep stations outside the blue hole (C3、C4)	187.18 ± 23.07	/	31.67 ± 7.60	10.06 ± 9.96	0.67 ± 0.54	4.99 ± 7.29	0.10 ± 0.09
Shallow stations outside the blue hole (C1、C2、C5)	194.22 ± 3.26	/	–	3.48 ± 0.64	0.14 ± 0.04	0.25 ± 0.26	0.05 ± 0.05

Note: Units for Oxidation–reduction potential (ORP), suspended particulate matter (SPM), methane (CH_4)/nitrous oxide (N_2O) and dissolved inorganic carbon (DIC) are mv, mg L^{-1}, nmol L^{-1} and μmol kg^{-1}, respectively; Units for other variables (except pH) are μmol L^{-1}; "/" represents undetectable level and "——" refers to untested.

from 15.0 to 2.4 μmol L^{-1}, and then increased with depth to 5.1 μmol L^{-1} at a depth of 75 m, changing little below 75 m. Concentrations of DOC were higher in the upper 100 m of the water column, but also exhibited great variability. Two DOC maxima were observed at depths of 30 m and 75 m, the latter caused by phytoplankton production coinciding with a peak in POC. Higher pH values were observed in the surface mixed layer, which was a phenomenon that was also observed in the blue hole (Fig. 6d). The value of pH reached a maximum at a depth of 50 m, and then decreased with greater depth. Concentrations of DIC were lower in the surface mixed layer and increased with depth. A similar distribution was found in the oxic water of the blue hole. Calculated pCO_2 increased with depth, and minimum pCO_2 coincided with maximum pH. Calculated values of Ω_{Ca} ranged from 2.06 to 4.85 and Ω_{Ar} varied between 1.32 and 3.24, suggesting that $CaCO_3$ is supersaturated in the water column (Fig. 7b).

4. Discussion

4.1. Chemical characteristics of the water column

The vertical stratification of the Sansha Yongle Blue Hole is controlled by temperature gradients, which is similar to the situation in the Cariaco Basin but contrasts with that of the Black Sea and Bahamas blue holes, where salinity gradients control the density structure (Scranton et al., 2001; Konovalov et al., 2008; Gonzalez et al., 2011). On the basis of redox state and chemical characteristics, the water column inside the blue hole can be divided into an oxic layer in the top 70 m, a chemocline at a depth of 70–100 m and an anoxic layer of deep water below a depth of 100 m. The statistic results of chemical variables in the three layers inside the blue hole as well as those outside the blue hole are listed in Table 1.

The mean levels of DO, pH and DIC measured in the upper oxic layer of the blue hole were lower than those measured outside the blue hole. Concentrations of nutrients (except for PO_4^{3-}), SPM, and N_2O in the blue hole were also higher than those measured at shallow stations outside the blue hole, but lower than those measured at deep stations outside the blue hole. Concentrations of POC measured inside the blue hole were similar to values measured at deep stations outside the blue hole, but lower than values measured at shallow stations outside the blue hole. Values of ORP and CH_4 measured inside the blue hole were similar to those measured at other stations (Table 1).

Estimates of both the saturation level and flux of N_2O were higher than those calculated for the surface waters outside the blue hole. Reported estimates of N_2O saturation levels and fluxes for other coastal and shelf areas (summarized in Table 2), exhibits great variability, ranging from 105% to 163% and 0.06 to 14.8 μmol m^{-2} d^{-1}, respectively. The saturation levels and fluxes of N_2O in the Sansha Yongle Blue Hole and the adjacent sea area were generally comparable to the values of the Black Sea reported by Amouroux et al. (2002). They were higher than those estimated for Caribbean Sea and the Arabian Sea, but lower than those estimated in the South China Sea (Morell et al., 2001; Lal et al., 1996; Zheng et al., 2009). Reported saturation levels and fluxes of CH_4 for other coastal and shelf areas also varied greatly, ranging from 58% to 10,500% and −27.9 to 120 μmol m^{-2} d^{-1}, respectively (Table 3). The estimated saturation levels and fluxes of CH_4 for the Sansha Blue Hole and the adjacent sea area fall within these ranges. More generally, the CH_4 flux from the Sansha Yongle Blue Hole in this study was lower than that estimated in the Black Sea, but much higher than those reported for other areas such as the Arabian Sea, North Sea and Yellow Sea (Amouroux et al., 2002; Patra et al., 1998; Zhang et al., 2004). In general, the surface waters of the blue hole and the adjacent sea area were supersaturated with N_2O and CH_4. Hence the blue hole behaves as a net source of N_2O and CH_4 to the atmosphere.

Profiles of nutrients, sulfide, pH, and DIC for the chemocline inside the Sansha Yongle Blue Hole were similar to those reported for the Black Sea and Baltic Sea (Jost et al., 2010; Yakushev et al., 2006), but were different from those reported for other blue holes characterized by a fresh water lens (Gonzalez, 2010). Concentrations of N_2O were much lower than those observed in other low-oxygen environments, such as the shelf off western India (533 nmol L^{-1}; Naqvi et al., 2000), and the eastern tropical South Pacific (173 nmol L^{-1}; Codispoti et al., 1992). The low N_2O concentration in the blue hole could be caused by lower production rates, higher consumption rates, or combination of these two processes.

Sulfide concentrations within the anoxic layer of the blue hole, were close to those reported for the Baltic Sea (25–50 μmol L^{-1}), the Cariaco Basin (~40 μmol L^{-1}), and the upper anoxic part (at a depth of ~200 m) of the Black Sea, but were much lower than reported values of sulfide concentrations measured in the deeper waters of the Black Sea (~425 μmol L^{-1}; Jost et al., 2010; Yakushev et al., 2006; Wakeham et al., 2012). Concentrations of NH_4^+, pH, and DIC in the anoxic layer of the blue hole were similar to those in the Black Sea. However, CH_4 concentrations were much lower than those reported for the Black Sea (~11 μmol L^{-1}) and the Cariaco Basin (~10 μmol L^{-1}) (Reeburgh et al., 1991; Wakeham et al., 2012).

Concentrations of DO, ORP, DOC, pH and N_2O were highest in the upper oxic layer of the Sansha Yongle Blue Hole and lowest in the deep anoxic layer. The deep anoxic layer had high concentrations of nutrients (SiO_3^{2-}, PO_4^{3-}, NH_4^+), DIC, and CH_4, which were dozens of times higher than those found in the upper water column. In contrast, concentrations of DO, NO_3^-, NO_2^- and N_2O in this layer were extremely low or at undetectable levels (Table 1).

4.2. Formation of the chemocline

Except for the surface water, seawater in the Sansha Blue Hole is disconnected from the sea outside the blue hole. This hydrodynamic condition leads to the formation of a strong permanent thermocline inside the blue hole that inhibits exchange between the surface and deep waters. Over thousands of years (about 6000 years according to the ^{14}C dating, unpublished data), dissolved oxygen has become depleted in the deeper water layers of the blue hole through the continued decomposition of particulate organic matter that sinks from the upper water column. Oxygen depletion led to anaerobic decomposition, which resulted in the production and accumulation of sulfide in the deep water. Therefore, a chemocline was formed in the permanent thermocline, with oxic water/sulfidic water above/below the chemocline. Within the chemocline, oxygen and sulfide coexist over a depth of ~20 m, a situation which contrasts with the absence of direct contact between sulfide and oxygen observed in the Black Sea (Murray et al.,

NH_4^+	SPM	DOC	POC	pH	DIC	CH_4	N_2O
0.83 ± 0.06	7.6 ± 4.92	105.84 ± 10.02	5.49 ± 2.26	7.99 ± 0.09	1969.37 ± 50.34	6.84 ± 0.98	7.86 ± 0.56
2.92 ± 3.12	20.33 ± 18.11	69.55 ± 4.35	6.25 ± 0.42	7.70 ± 0.04	2246.21 ± 117.03	56.73 ± 69.25	5.82 ± 3.60
74.92 ± 39.92	6.19 ± 3.30	71.87 ± 12.52	4.93 ± 0.52	7.55 ± 0.06	2888.45 ± 307.64	1733.34 ± 1091.73	2.09 ± 1.58
0.74 ± 0.10	9.58 ± 2.40	93.6 ± 65.0	5.88 ± 2.35	8.06 ± 0.08	2021.02 ± 81.06	7.73 ± 5.23	9.81 ± 3.36
0.82 ± 0.16	5.51 ± 5.83	92.24 ± 0.11	9.47 ± 30.9	8.12 ± 0.02	1921.11 ± 5.89	6.84 ± 3.81	6.84 ± 0.29

1989). Observations from many other anoxic seas and blue holes demonstrate that complicated oxidation–reduction reactions occur within the chemocline (Murray et al., 1995; Gonzalez, 2010; Yakushev et al., 2006).

The stability of the interface of chemocline is maintained by anaerobic sulfide oxidation coupled with nitrogen transformations. The upward flux of sulfide at the depth of its onset is considered to be equal to its production rate in the anoxic layer. Therefore, sulfide oxidation is assumed to take place at the lower boundary of the oxic water, where oxygen diffusing downward forms a layer of coexisting oxygen and sulfide (Konovalov et al., 2001). The half time for sulfide oxidation by oxygen is approximately one day and can be much shorter if the process of sulfide oxidation is catalyzed by dissolved trace metals (Iii et al., 1991). It is assumed that oxidation takes place at a minimum oxygen concentration of 2 μmol L^{-1}, and reaches maximum efficiency at concentrations above 9 μmol L^{-1} (Oguz et al., 2001). A continuous supply of oxygen is required to maintain the process of sulfide oxidation. However, as oxygen is depleted below a depth of 90 m inside the blue hole, the interface of the chemocline must be maintained by other processes in addition to oxidation reactions by oxygen. Sulfide and NH_4^+ are also oxidized by high valence metallic ions (e.g. Mn^{4+}, Mn^{3+} and Fe^{3+}) (Oguz et al., 2001). Meanwhile, NH_4^+ is oxidized by NO_2^- via anammox reaction (Kuypers et al., 2003), and NO_3^- is reduced to nitrogen (N_2) via denitrification. Although these oxidation–reduction reactions are typically catalyzed by microorganisms, the presence of dissolved chemicals may also play a role. Konovalov and Murray (2001) showed that, in the Black Sea, >50% of the upward flux of sulfide could be directly oxidized by oxygen and particulate manganese.

Anaerobic photosynthesis may be another mechanism contributing to the oxidation–reduction dynamics in the chemocline. The sulfide interface of the blue hole is located at depths of 80–100 m, where enough light can maintain bacterial photosynthetic activity. The suboxic layer contains high concentrations of bacteriochlorophyll that are roughly 3 times higher than those measured in the upper water column (unpublished data). This suggests the presence of large quantities of bacteria in the chemocline, including species such as *Chlorobi* that are capable of growing under very low light conditions and oxidize reduced sulfur compounds (H_2S or S^0) during photosynthesis (Oguz et al., 2001; Gonzalez et al., 2011). The reduced chemical species (e.g., HS^-, Mn^{2+} and Fe^{2+}) may also be oxidized by anaerobic phototrophic bacteria in association with phototrophic reduction of CO_2 to organic matter. Repeta and Simpson (1991) discovered large quantities of bacteriochlorophyll pigments near the suboxic–anoxic boundary of the Black Sea, providing support for this mechanism.

Table 2
Compilation of N_2O measurements in various coastal and shelf areas.

Study area	Stations	Date	Wind speed m s^{-1}	Surface N_2O concentration nmol L^{-1}	Surface N_2O saturation %	Sea-air N_2O fluxes μmol m^{-2} d^{-1}	Reference
Shelf of NW Black Sea	55	July-Aug. 1995		7.9 ± 0.8	112	2.7[a] 4.4[b]	Amouroux et al., 2002
Caribbean Sea	3	April 1995	7.9 ± 1.1	6.60 ± 0.6	114 ± 9	0.069 ± 0.070[a]	Morell et al., 2001
Arabian Sea	5	April–May 1994			105 ± 8	0.06 ± 0.79[a]	Lal et al., 1996
South China Sea	23	April–May 2005		9.6 ± 3.0	162.8 ± 45.4	9.07 ± 11.24[a] 14.8 ± 18.07[b]	Zheng et al., 2009
The blue hole and adjacent sea area	5	May 2017	6.98 ± 0.88	6.95 ± 0.32	121.4 ± 5.62	3.8 ± 0.87[a] 5.6 ± 1.52[b]	This study

[a] K_w was estimated by the LM86 equations.
[b] K_w was estimated by the W92 equation.

Table 3
Compilation of CH_4 measurements in various coastal and shelf areas.

Study area	Stations	Date	Wind speed m s^{-1}	Surface CH_4 concentration nmol L^{-1}	Surface CH_4 saturation %	Sea-air CH_4 flux μmol m^{-2} d^{-1}	Reference
NW Black Sea	80	July–Aug. 1995		13.1 ± 10.6	173–10,500	32[a]; 53[b]	Amouroux et al., 2002
Arabian Sea	11	April–May 1994			140 ± 37	0.032 ± 0.162[a]	Patra et al., 1998
North Sea	216	May 1994	8.0 ± 0.20		215 ± 75.4c	15.1 ± 10.7[b]	Rehder et al., 1998
Yellow Sea	14	Mar–Apr 2001	6.3 ± 2.1	3.43 ± 0.23	121 ± 5.4	0.81 ± 0.50[a] 1.33 ± 0.76[b]	Zhang et al., 2004
South China Sea	81	Apr–May 2010	0.14–19.5	1.15–5.6	59.7−298.8	−17.7–61.3[a] −27.9–119.6[b]	Ma and Chui, 2013
The blue hole and adjacent sea area	5	May 2017	6.98 ± 0.88	6.92 ± 1.13	369 ± 58.2	15.5 ± 2.97[a] 22.9 ± 5.24[b]	This study

[a] K_w was estimated by the LM86 equations.
[b] K_w was estimated by the W92 equation.

4.3. Nitrogen transformation

The distinct redox systems that dominate inorganic nutrient cycling and remineralization of organic matter between the surface oxic layer, chemocline and deep anoxic layer result in complex interactions between physical and biological processes (Murray et al., 1995; Oguz, 2005).

In the oxic layer (at depths of 0–70 m), assimilation is the dominant process whereby DIN is converted to organic nitrogen by phytoplankton or coralline symbiotic algae, resulting in very low or even undetectable levels of DIN above the seasonal thermocline. However, below the seasonal thermocline, nitrification resulted in NO_2^- release at a depth of 30 m, creating the primary nitrite maximum (Lomas and Fredric, 2006). Nitrification also led to the increase of nitrate. In the oxic layer but below the euphotic zone (at depths of 50–70 m), the main biological processes are likely to have shifted to nitrification and mineralization catalyzed by microorganisms, as NO_3^- concentrations increase with decreasing DO, reaching a maximum value at lower DO concentrations (<150 μmol L^{-1}).

Within the chemocline (at depths of 70–100 m), a sharp reduction in NO_3^- concentrations are accompanied by an increase in NO_2^- concentrations due to denitrification. Meanwhile, N_2O concentrations decrease to very low level in the suboxic zone, indicating net consumption. Nitrite is reduced to N_2 at the upper boundary of the anoxic layer due to anammox reactions ($NO_2^- + NH_4^+ \rightarrow N_2$) (Kuypers et al., 2003) (Fig. 4 a, Fig. 5 a). Denitrification has been considered as an important sink of marine-fixed nitrogen, especially before anammox processes were discovered (Brandes and Devol, 2002). However, nitrogen loss (N-loss) in the suboxic layer of the Black Sea or in other oceanic oxygen minimum zones can only be explained by the dominance of anammox (Konovalov et al., 2008; Hamersley et al., 2007). Unfortunately, we are unable to quantify the balance between anammox and denitrification in the Sansha Yongle Blue Hole and therefore proceed to provide an estimate of N-loss. The theoretical nitrogen (N): phosphorus (P) ratio in oxic or anoxic environments has been reported to be 16:1, assuming that the source of these nutrients is the decomposition of organic matter (Redfield et al., 1963; Richards, 1965; Hiscock and Millero, 2006). In the chemocline inside the blue hole, we measured a N:P ratio of <16:1. A minimum value of 6.7 was observed in the suboxic layer, indicating that nitrogen removal mainly occurs within this layer. Assuming that the N:P ratio follows the stoichiometric ratio, N-loss in the suboxic layer was estimated to be 60% based on the measured N:P ratio.

All nitrogen oxides are depleted in the upper part of the anoxic zone (at depths of 100–125 m). Meanwhile, NH_4^+ accounts for >99.9% of DIN in the anoxic deep water (below 100 m) as a result of the ammonification of particulate organic nitrogen (Ward and Kilpatrick, 1991). A similar nitrogen cycle was observed in the Black Sea (Murray et al., 1995).

4.4. Organic carbon and the carbonate system

Carbon cycling in the Sansha Yongle Blue Hole differs significantly from carbon cycling in most other coastal seas and the open ocean due to the presence of a predominantly anoxic water column. Photosynthesis results in uptake of CO_2, decreases in DIC and pCO_2, and an increase in pH. This is accompanied by a shift in the carbonate system, reducing the concentration of bicarbonate (HCO_3^-). In contrast, oxidation of organic carbon increases DIC and supports acidification (Goyet et al., 1991).

We initially supposed that pH in the upper oxic euphotic zone of the blue hole would increase, as nutrients facilitate primary production processes. However, our observations indicate that pH and DO both decrease, while DIC, pCO_2 and POC all increase in the subsurface layer (at a depth of 30 m) (Fig. 6a, Fig. 7a). This may indicate that while both photosynthesis and organic matter oxidation are the main biological and chemical processes, the latter is the dominant process controlling the chemistry of the upper oxic euphotic zone. In the oxic layer but below the euphotic zone, decomposition of POC and release of DOC by heterotrophic bacteria may cause increases in DOC, DIC and pCO_2, and decreases in POC and pH (Fig. 6a, Fig. 7a).

While oxidative degradation or aerobic respiration of bacteria is restricted to the oxic layer, mineralization of organic matter extends beyond the oxic layer. Organic matter from the upper water column sinks to the suboxic zone, resulting in higher DIC and lower pH. As a result of oxygen depletion, bacterial metabolism shifts from aerobic to anaerobic respiration (Ducklow et al., 2007; Morgan et al., 2006). Bacteria use other oxidants (e.g. NO_3^-, MnO_2, FeOOH) in a stepwise progression based on the decreased energy yield from the reactions (Morgan et al., 2006).

Within the anoxic layer, the increases in pCO_2 and DIC in the upper anoxic water reflect the net effect of all oxidation–reduction reactions on the carbon and proton balances. The main chemical reactions involved in the change of DIC, pCO_2, and organic carbon result from oxidation of organic matter by means of sulfate reduction (Konovalov et al., 2001). Bacterial primary production within the blue hole may contribute significantly to the blue hole food web and result in accumulations of DOC at a depth of 150 m (Ducklow et al., 2007). In addition, considering the low saturation state of aragonite ($\Omega_{Ar} = \sim 1$), dissolution of $CaCO_3$ is likely to have contributed to the increase of DIC and pCO_2. In the deeper anoxic water, concentrations of carbonate system components remain constant or vary little, confirming the relatively steady state of the deeper water.

5. Conclusion

The water column of the Sansha Yongle Blue Hole is stratified by two thermoclines and divided into five distinct layers: the upper mixed layer in the top 13 m, the seasonal thermocline at depths of 13–20 m, the week mixing layer at depths of 20–70 m, the permanent thermocline at depths of 70–150 m, and the homogeneous deep water below a depth of 150 m. A 30-m thick chemocline that acts as a redox boundary separates the upper oxic layer (the top 70 m) from the deep anoxic layer (below 100 m). DO decreases with depth and is depleted in the chemocline at a depth of about 100 m. A subsurface oxygen minimum is observed due to oxidation of organic matter, whereas the oxygen maximum at the bottom of the euphotic layer is most likely caused by photosynthesis. Within the chemocline, oxygen decreases sharply to undetectable levels, whereas sulfide is detectable below a depth of 80 m, but remains low throughout the chemocline. Sulfide increases almost linearly from the upper boundary of the anoxic layer to the depth of 150 m and maintains high value to the bottom of the water column. ORP is positive in the oxic layer, but changes sharply to negative values in the chemocline and anoxic water.

Distinct redox systems involve different nitrogen transformation processes. DIN was depleted in the upper mixed layer due to biological uptake, but nitrification is the main biological process below the seasonal thermocline, resulting in an increase in nitrate and the formation of the primary nitrite maximum. Within the chemocline, denitrification results in a sharp decrease in nitrate overall and peak values of nitrite and nitrous oxide at a depth of 90 m, and ammonium starts to increase because of the mineralization of organic carbon. Nitrogen removal mainly occurs in the chemocline and about 60% of the nitrogen is lost via denitrification and anammox. In the deep anoxic water, ammonium is the only form of DIN.

The carbon cycle in the Sansha Yongle Blue Hole is closely related to the redox environment and biological activity. Within the euphotic zone (except at a depth of around 30 m), photosynthesis is the dominant biological process, leading to increases in oxygen and pH and transformation of inorganic carbon into organic carbon. Below the euphotic zone, organic matter degradation is the main biologic process, leading to a decrease in pH and an increase in DIC. Within the chemocline, carbon transformation processes are governed by microbial activity. Organic matter mineralization results in a sharp decrease in pH, DOC and an

increase in DIC, whereas organic matter produced in situ by chemoautotrophic and photoautotrophic microorganisms leads to a peak in POC concentrations. In the anoxic deep water, organic matter consumption exceeds production, leading to decreases in POC and pH and an increase in DIC. In addition, considering the low saturation state of aragonite ($\Omega_{Ar} = \sim 1$), dissolution of $CaCO_3$ is likely to have contributed to the increase of DIC and pCO_2. In the deeper anoxic water, concentrations of carbon variables maintain nearly constant levels, confirming the relatively steady state of the deep water.

The unique hydro-biochemical nature of the Sansha Yongle Blue Hole provides an interesting and challenging site for revealing fundamental processes of biogeochemical cycling and for deducing paleoenvironment and paleoclimates. This research is helpful for understanding the distinct redox systems that dominate inorganic nutrient dynamics and carbon cycling, resulting in complex interactions between physical and biological processes. Further studies should be carried out to identify the roles of the redox-sensitive metals (e.g., Mn^{2+}, Mn^{3+} and Fe^{3+}) and microorganism on the coupled cycles of carbon, nitrogen and sulfur, including the aerobic/anaerobic oxidation processes of dissolved Mn (II, III) and ammonium, nitrate removal by denitrification and POM synthesis by chemoautotrophic production within the chemocline and deep anoxic bottom water.

Acknowledgments

We thank professor Guiling Zhang from Ocean University of China for the determination of N_2O and CH_4. We acknowledge staff of China Offshore Fugro Geosolutions (Shenzhen) Co., Ltd. for their support in sample collection by ROV. We thank many persons for their support and/or assistance with our research, particularly Sangyun Wu, Yanxiong Liu, Jun Du, Li Li, Liang Xue, Daolong Wang, Chao Yuan, Xia Sun, Ying Wang, Kan Chen, Hanyue Xu. We thank Tina Tin, PhD, and Guy Evans, PhD, from Liwen Bianji, Edanz Group China (www.liwenbianji.cn/ac), for editing the English text of a draft of this manuscript. This work was funded by grants from the Global Change and Air–Sea Interaction Program (GASI-01-01-01-23) and the Basic Scientific Fund for National Public Research Institutes of China (GY0217Y02, 2016Q08).

References

Amouroux, D., Roberts, G., Rapsomanikis, S., Andreae, M.O., 2002. Biogenic gas (CH, NO, DMS) emission to the atmosphere from near-shore and shelf waters of the Northwestern Black Sea. Estuar. Coast. Shelf Sci. 54, 575–587.

Brandes, J.A., Devol, A.H., 2002. A global marine-fixed nitrogen isotopic budget: Implications for Holocene nitrogen cycling. Glob. Biogeochem. Cycles 16 (67-61-67-14).

Cai, W.J., Wang, Y., 1998. The chemistry, fluxes, and sources of carbon dioxide in the estuarine waters of the Satilla and Altamaha Rivers, Georgia. Limnol. Oceanogr. 43, 657–668.

Chen, C.T.A., Wang, S.L., Wang, B.J., Pai, S.C., 2001. Nutrient budgets for the South China Sea basin. Mar. Chem. 75, 281–300.

Codispoti, L.A., Elkins, J.W., Yoshinari, T., Friederich, G.E., Sakamoto, C.M., Packard, T.T., 1992. On the Nitrous Oxide Flux From Productive Regions That Contain Low Oxygen Waters. pp. 271–284.

Dickson, A.G., 1990. Standard potential of the reaction: ja:math, and and the standard acidity constant of the ion HSO_4^- in synthetic sea water from 273.15 to 318.15 K. J. Chem. Thermodyn. 22, 113–127.

Ducklow, H.W., Hansell, D.A., Morgan, J.A., 2007. Dissolved organic carbon and nitrogen in the Western Black Sea. Mar. Chem. 105, 140–150.

Fanning, K.A., Pilson, M., 1973. On the spectrophotometric determination of dissolved silica in natural waters. Anal. Chem. 45, 136–140.

Flynn, E.D., 2013. Carbon and Oxygen Isotope Study of Carbonates From Watling's Blue Hole and Blue Hole Five, San Salvador, Bahamas, World of Lakes. Western Kentucky University, America, p. 427.

Gischler, E., 2011. Blue Hole. Encyclopedia of Earth Sciences pp. 164–165.

Gonzalez, B.C., 2010. Novel Bacterial Diversity in an Anchialine Blue Hole on Abaco Island, Bahamas. Texas A&M University, America, pp. 16–18.

Gonzalez, B.C., Iliffe, T.M., Macalady, J.L., Schaperdoth, I., Kakuk, B., 2011. Microbial hotspots in anchialine blue holes: initial discoveries from the Bahamas. Hydrobiologia 677, 149–156.

Goyet, C., Bradshaw, A.L., Brewer, P.G., 1991. The carbonate system in the Black Sea. Deep Sea Res. Part A 38, S1049–S1068.

Hamersley, M.R., Lavik, G., Woebken, D., Rattray, J.E., Lam, P., Hopmans, E.C., Damsté, J.S.S., Krüger, S., Graco, M., Gutiérrez, D., 2007. Anaerobic ammonium oxidation in the Peruvian oxygen minimum zone. Limnol. Oceanogr. 52, 923–933.

Hatcher, B.G., 2006. Origin of Blue Hole Structures in Coral Reefs: Houtman Abrolhos, Western Australia. J. Coast. Res. 22, 202–208.

Hiscock, W.T., Millero, F.J., 2006. Alkalinity of the anoxic waters in the Western Black Sea. Deep-Sea Res. II Top. Stud. Oceanogr. 53, 1787–1801.

Iii, G.W.L., Church, T.M., Powell, D., 1991. Sulfur speciation and sulfide oxidation in the water column of the Black Sea. Deep Sea Res. Part A 38, S1121–S1137.

Jost, G., Martens-Habbena, W., Pollehne, F., Schnetger, B., Labrenz, M., 2010. Anaerobic sulfur oxidation in the absence of nitrate dominates microbial chemoautotrophy beneath the pelagic chemocline of the eastern Gotland Basin, Baltic Sea. FEMS Microbiol. Ecol. 71, 226.

Kjellmark, E., 1996. Late Holocene climate change and human disturbance on Andros Island, Bahamas. J. Paleolimnol. 15, 133–145.

Konovalov, S.K., Murray, J.W., 2001. Variations in the chemistry of the Black Sea on a time scale of decades (1960–1995). J. Mar. Syst. 31, 217–243.

Konovalov, S.K., Ivanov, L.I., Samodurov, A.S., 2001. Fluxes and budget of sulphide and ammonia in the Black Sea anoxic layer. J. Mar. Syst. 31, 203–216.

Konovalov, S.K., Fuchsman, C.A., Belokopitov, V., Murray, J.W., 2008. Modeling the distribution of nitrogen species and isotopes in the water column of the Black Sea. Mar. Chem. 111, 106–124.

Kuypers, M.M., Sliekers, A.O., Lavik, G., Schmid, M., Jørgensen, B.B., Kuenen, J.G., Sinninghe Damsté, J.S., Strous, M., Jetten, M.S., 2003. Anaerobic ammonium oxidation by anammox bacteria in the Black Sea. Nature 422, 608.

Lal, S., Patra, P.K., Venkataramani, S., Sarin, M.M., 1996. Distribution of Nitrous Oxide and Methane in the Arabian Sea.

Liss, P.S., Merlivat, L., 1986. Air-sea gas exchange rates: introduction and synthesis. The Role of Air-sea Exchange in Geochemical Cycling. 185, pp. 113–127.

Lomas, M.W., Fredric, L., 2006. Forming the primary nitrite maximum: nitrifiers or phytoplankton? Limnol. Oceanogr. 51, 2453–2467.

Lueker, T., Dickson, A., Keeling, C., 2000. Ocean pCO_2 calculated from dissolved inorganic carbon, alkalinity, and equations for K1 and K2: validation based on laboratory measurements of CO_2 in gas and seawater at equilibrium. Mar. Chem. 70, 105–119.

Ma, L.J., Chui, Y.C., 2013. Dissolved methane concentration and sea-to-air transfer flux of dissolved methane in the upper seawater of the central and northern South China Sea. J. Trop. Oceanogr. 32, 94–101.

Macalady, J.L., Dattagupta, S., Schaperdoth, I., Druschel, G.K., Eastman, D., 2008. Niche differentiation among sulfuroxidizing bacterial populations in cave waters. Iseme J. 2, 590–601.

Martin, J.B., Gulley, J., Spellman, P., 2012. Tidal pumping of water between Bahamian blue holes, aquifers, and the ocean. J. Hydrol. 416–417, 28–38.

Morell, J.M., Capella, J., Mercado, A., Bauzá, J., Corredor, J.E., 2001. Nitrous oxide fluxes in Caribbean and tropical Atlantic waters: evidence for near surface production. Mar. Chem. 74, 131–143.

Morgan, J.A., Quinby, H.L., Ducklow, H.W., 2006. Bacterial abundance and production in the western Black Sea. Deep-Sea Res. II Top. Stud. Oceanogr. 53, 1945–1960.

Murphy, J., Riley, J.P., 1962. A modified single solution method for the determination of phosphate in natural waters. Anal. Chim. Acta 27, 31–36.

Murray, J.W., Jannasch, H.W., Honjo, S., Anderson, R.F., Reeburgh, W.S., Top, Z., Friederich, G.E., Codispoti, L.A., Izdar, E., 1989. Unexpected changes in the oxic/anoxic interface in the Black Sea. Nature 338, 411–413.

Murray, J.W., Codispoti, L.A., Friederich, G.E., 1995. Oxidation-reduction environments: the suboxic zone in the Black Sea. In: Huang, C.P., O'melia, C.R., Morgan, J.J. (Eds.), Aquatic Chemistry:Interfacial and Interspecies Precosses ACS Advances in Chemistry Series No 224, pp. 157–176.

Mylroie, J.E., Carew, J.L., Moore, A.I., 1995. Blue holes: definition and genesis. Carbonates Evaporites 10, 225–233.

Naqvi, S.W.A., Jayakumar, D.A., Narvekar, P.V., Naik, H., Sarma, V.V.S.S., D'souza, W., Joseph, S., George, M.D., 2000. Increased marine production of N_2O due to intensifying anoxia on the Indian continental shelf. Nature 408, 346–349.

Naumann, M.S., Bednarz, V.N., Ferse, S.C., Niggl, W., Wild, C., 2015. Monitoring of coastal coral reefs near Dahab (Gulf of Aqaba, Red Sea) indicates local eutrophication as potential cause for change in benthic communities. Environ. Monit. Assess. 187, 44.

Oguz, T., 2005. Black Sea ecosystem response to climatic teleconnections. Oceanography 18, 122–133.

Oguz, T., Murray, J.W., Callahan, A.E., 2001. Modeling redox cycling across the suboxic–anoxic interface zone in the Black Sea. Deep-Sea Res. I Oceanogr. Res. Pap. 48, 761–787.

Patra, P.K., Lal, S., Venkataramani, S., Gauns, M., Sarma, V.V.S.S., 1998. Seasonal variability in distribution and fluxes of methane in the Arabian Sea. J. Geophys. Res. Oceans. 103, 1167–1176.

Pierrot, D., Lewis, E., Wallace, R., Wallace, D., Wallace, W., Wallace, D.W.R., 2006. MS Excel Program Developed for CO_2 System Calculations.

Pohlman, J.W., Iliffe, T.M., Cifuentes, L.A., 1997. A stable isotope study of organic cycling and the ecology of an anchialine cave ecosystem. Mar. Ecol. Progress. 155, 17–27.

Redfield, A.C., Ketchum, B.H., Richards, F.A., 1963. The influence of organisms on the composition of sea-water. In: Hill, M.N. (Ed.), The Sea. Interscience, New York, pp. 26–27.

Reeburgh, W.S., Ward, B.B., Whalen, S.C., Sandbeck, K.A., Kilpatrickt, K.A., Kerkhof, L.J., 1991. Black Sea methane geochemistry. Deep Sea Res. Part A 38, S1189–S1210.

Rehder, G., Keir, R.S., Suess, E., Pohlmann, T., 1998. The multiple sources and patterns of methane in North Sea Waters. Aquat. Geochem. 4, 403–427.

Repeta, D.J., Simpson, D.J., 1991. The distribution and recycling of chlorophyll, bacteriochlorophyll and carotenoids in the Black Sea. Deep Sea Res. Part A 38, S969–S984.

Richards, F.A., 1965. Anoxic basins and fjords. In: Riley, J.P., Skirrow, G. (Eds.), Chemical Oceanography. Academic Press, New York, pp. 611–646.

Schwabe, S., Herbert, R.A., 2004. Black Holes of the Bahamas: what they are and why they are black. Quat. Int. 121, 3–11.

Scranton, M.I., Astor, Y., Bohrer, R., Ho, T.Y., Muller-Karger, F., 2001. Controls on temporal variability of the geochemistry of the deep Cariaco Basin. Deep-Sea Res. I Oceanogr. Res. Pap. 48, 1605–1625.
Seymour, J.R., Humphreys, W.F., Mitchell, J.G., 2007. Stratification of the microbial community inhabiting as anchialine sinkhole. Aquat. Microb. Ecol. 50, 11–24.
State technology supervision bureau. GB 17378.4-2007, 2007. The Specification Formarine Monitoring. Part4: Seawater Analysis. Standards Press of China, Beijing, China.
Strickland, J.D.H., Parsons, T.R., 1972. A practical handbook of seawater analysis. Bulletin 167.
Su-Cheng, P., Yang, C.C., Riley, J.P., 1990. Effects of acidity and molybdate concentration on the kinetics of the formation of the phosphoantimonylmolybdenum blue complex. Anal. Chim. Acta 229, 115–120.
Sugimura, Y., Suzuki, Y., 1988. A high-temperature catalytic oxidation method for the determination of non-volatile dissolved organic carbon in seawater by direct injection of a liquid sample. Mar. Chem. 24, 105–131.
Uppström, L.R., 1974. The boron/chlorinity ratio of deep-sea water from the Pacific Ocean. Deep-Sea Res. Oceanogr. Abstr. 21, 161–162.
Vermette, S., Hudson, R., 2001. Hydrology of watling's blue hole: san salvador, bahamas. Middle States Geographer. 34, 55–62.
Wakeham, S.G., Turich, C., Schubotz, F., Podlaska, A., Li, X.N., Varela, R., Astor, Y., Sáenz, J.P., Rush, D., Damsté, J.S.S., 2012. Biomarkers, chemistry and microbiology show chemoautotrophy in a multilayer chemocline in the Cariaco Basin. Deep-Sea Res. Part I 63, 133–156.
Wanninkhof, R., 1992. Relationship between wind speed and gas exchange over the ocean. J. Geophys. Res. Oceans. 97, 7373–7382.
Ward, B.B., Kilpatrick, K.A., 1991. Nitrogen transformations in the oxic layer of permanent anoxic basins: the Black Sea and the Cariaco Trench. Black Sea Oceanography. Springer, Netherlands, pp. 111–124.
Weiss, R.F., Price, B.A., 1980. Nitrous oxide solubility in water and seawater. Mar. Chem. 8, 347–359.
Wiesenburg, D.A., Gulnasso Jr., N.L., 1979. Equilibrium solubilities of methane, carbon monoxide, and hydrogen in water and sea water. J. Chem. Eng. Data 24, 356.
Yakushev, E.V., Chasovnikov, V.K., Debolskaya, E.I., Egorov, A.V., Makkaveev, P.N., Pakhomova, S.V., Podymov, O.I., Yakubenko, V.G., 2006. The northeastern Black Sea redox zone: Hydrochemical structure and its temporal variability. Deep-Sea Res. II Top. Stud. Oceanogr. 53, 1769–1786.
Zhang, G.L., Zhang, J., Kang, Y.B., Liu, S.M., 2004. Distributions and fluxes of methane in the East China Sea and the Yellow Sea in spring. J. Geophys. Res. Oceans. 109.
Zhang, G.L., Zhang, J., Xu, J., Zhang, F., 2006. Distributions, sources and atmospheric fluxes of nitrous oxide in Jiaozhou Bay. Estuar. Coast. Shelf Sci. 68, 557–566.
Zheng, L.X., Zhang, G.L., Xu, J., Zhang, F., Zhang, J., 2009. Distribution and air-sea fluxes of N_2O in South China Sea in spring. Mar. Environ. Sci. 3, 233–237.